JOURNAL OF Applied Polymer SCIENCE

# Study on the Preparation of Eu(Pht)$_3$Phen/SBA-15 Hybrids and Photoluminescence Properties of Silicone Rubber Composites with the Hybrids

**Shengjie Xu, Wentan Ren, Yong Zhang, Yinxi Zhang**
School of Chemistry and Chemical Engineering, Shanghai Jiao Tong University, Shanghai 200240, China
Correspondence to: W. Ren (E-mail: 1958rwt@sjtu.edu.cn)

**ABSTRACT:** In this work, Eu(Pht)$_3$Phen/SBA-15 hybrids were prepared by solution mixing and their morphologies and structures were characterized by X-ray diffraction (XRD), scanning electronic microscopy (SEM), nitrogen adsorption–desorption and transmission electronic microscopy (TEM). The results showed that Eu(Pht)$_3$Phen was successfully incorporated into the channels and assembled onto the surface of SBA-15 and the long range ordered structure of SBA-15 was preserved. The silicone rubber composites with Eu(Pht)$_3$Phen/SBA-15 hybrids were obtained by mechanical blending, and their morphologies and photoluminescence properties were studied. The results showed that the photoluminescence intensities of the composites with the hybrids increased as the content of the hybrids increased. The composite with the hybrids showed higher photoluminescence intensity and longer lifetime compared to the silicone rubber compounded with Eu(Pht)$_3$Phen (Eu(Pht)$_3$Phen/silicone rubber composite), Eu(Pht)$_3$Phen and SBA-15 ([Eu(Pht)$_3$Phen+SBA-15]/silicone rubber composite). Judd-Ofelt theory was used to investigate the local environment of $Eu^{3+}$ ions in the silicone rubber composites. The photoluminescence quantum efficiency of the silicone rubber composite with Eu(Pht)$_3$Phen/SBA-15 hybrids was calculated to be 31.0%, higher than that of Eu(Pht)$_3$Phen/silicone rubber composite (26.4%) and [Eu(Pht)$_3$Phen+SBA-15]/silicone rubber composite (25.4%). The enhancement in photoluminescence intensity and increase in lifetime and photoluminescence quantum efficiency could be attributed to the rigid structure of SBA-15 which reduced the nonradiative transition rate and the improvement of the dispersion of the hybrids in the composites. © 2012 Wiley Periodicals, Inc. J. Appl. Polym. Sci. 000: 000–000, 2012

**KEYWORDS:** Eu(Pht)$_3$Phen/SBA-15 hybrids; silicone rubber composites; photoluminescence properties; Judd-Ofelt theory

Received 4 April 2012; accepted 30 June 2012; published online
**DOI: 10.1002/app.38280**

## INTRODUCTION

Rare earth complexes have found potential applications in display, biomedical molecular probes and light emitting materials[1–4] due to their distinct photoluminescence properties of strong luminescence intensity, long lifetime, large Stokes shift, and sharp emission profile.[2,5] It was well established that the dispersion of rare earth complexes had played a vital role in the photoluminescence properties.[6] Rare earth complex/inorganic material hybrids have attracted much attention because of the improvement in the dispersion of rare earth complexes in the matrix.[7–9] Mesoporous silica materials possessed advantages of great surface area, rigid framework and long range ordered structure, making them promising hosts for rare earth complexes.[10–13] The rigid framework could both protect and stabilize the rare earth complexes.[8] Therefore, photostability under UV radiation, lifetime, and photoluminescence quantum efficiency could be improved owning to the enhanced energy transfer from ligand to metal ions.[14] Xu et al. reported the incorporation of rare earth complexes into the surface-modified mesoporous MCM-41 by hydrogen-bonding, which found that the incorporated rare earth complexes showed higher UV stability and longer lifetime compared to the pure complexes.[10] Compared with MCM-41, SBA-15, first synthesized by Zhao et al.,[15] was characterized of much larger pore size (up to 30 nm), thicker wall, and better stability,[12,16] which made it a promising host for rare earth complexes.

The rare earth complex/polymer composites with photoluminescence properties have been widely studied since that they not only possessed distinct photoluminescence properties but also with excellent processing ability, chemical stability, and mechanical strength,[17] which made them possible applications in display, probes, and laser materials.[18] Liu et al. reported the preparation and luminescent properties of cured and uncured samarium tris-(2-thenoltrifluoroacetone)-1, 10-phenanthroline/

nitrile rubber, which found that the luminescent intensity of cured composite was stronger than that of the uncured one because of the stabilization effect of the crosslinking network structure.[19] Wen et al. synthesized $Sm(TTA)_2(AA)(Phen)$ and prepared the $Sm^{3+}$ complex/HXNBR (hydrogenated carboxylated nitrile butadiene rubber) composite by *in situ* reaction and found that the cured composites exhibited higher photoluminescence intensity and longer photoluminescence lifetime compared to the uncured composites.[18] However, the preparation and photoluminescence properties of polymer composites compounded with rare earth complex/mesoporous material hybrids were rarely studied. While most of the studies focused on the photoluminescence intensity, few studies paid attention to the lifetime and photoluminescence quantum efficiency of the rare earth complex/polymer composites which were essential for the applications of the polymer composites.

Herein, $Eu(Pht)_3Phen$ and SBA-15 were synthesized and $Eu(Pht)_3Phen$/SBA-15 hybrids were prepared by solution mixing of $Eu(Pht)_3Phen$ and SBA-15. Their morphologies and structures were characterized by XRD, nitrogen adsorption–desorption, SEM, and TEM. The silicone rubber composites with $Eu(Pht)_3Phen$/SBA-15 hybrids were prepared by mechanical blending of various contents of $Eu(Pht)_3Phen$/SBA-15 hybrids with silicone rubber. Silicone rubber composites containing $Eu(Pht)_3Phen$ ($Eu(Pht)_3Phen$/silicone rubber composite), $Eu(Pht)_3Phen$ and SBA-15 ([$Eu(Pht)_3Phen$+SBA-15]/silicone rubber composite, which were prepared by direct mechanical blending of $Eu(Pht)_3Phen$ and SBA-15 separately), were also prepared by the same method for comparison. The morphologies and photoluminescence properties of the composites were investigated. Judd-Ofelt theory was used to investigate the local environment of the $Eu^{3+}$ ions in the composites, and photoluminescence quantum efficiency was also calculated.

## EXPERIMENTAL

### Materials

Silicone rubber (110-2, ethylene group content 0.13–0.20%, volatile component less than 0.25%) was produced from East Asia Polymer Materials Plant, Jilin, China. Europium oxide ($Eu_2O_3$, 99%) was purchased from Shanghai Yuelong Rare Earth New Materials, China. Poly(ethylene glycol)-*b*-poly(propylene glycol)-*b*–poly (ethylene glycol) (Pluronic P123, $M_w = 5800$) was supplied by Sigma-Aldrich (Shanghai) Trading Co. Ltd. 1,10-phenanthroline (1,10-Phen), potassium hydrogen phthalate (KHPht), dicumyl peroxide (DCP, analytical reagent grade) and tetraethoxysilane (TEOS) were supplied Sinopharm Chemical Reagent Co. Ltd., China. All the agents were used as received.

### Preparation of $Eu(Pht)_3Phen$/SBA-15 Hybrids

$Eu(Pht)_3Phen$ was synthesized through the reaction of $EuCl_3$, 1,10-Phen, and KHPht in a molar ratio of 1:1:3. 10 mmol of $Eu_2O_3$, 18 mL of HCl, and 18 mL of $H_2O$ were mixed at 85°C with magnetic stirring for 3 h, followed by continued heating to remove the remaining HCl. Then, 60 mmol of KHPht, 30 mL of ethanol, and 30 mL of $H_2O$ were added to the solution and reacted for 1 h. After that, 20 mmol of 1,10-Phen, 18 mL of ethanol, and 18 mL of $H_2O$ were mixed with the solution and reacted for 8 h. After the above mixture was cooled to room temperature, ammonia water (35 wt. %) was added to the solution to adjust the pH to 6–7 for precipitation, followed by filtration and extensive washing with water and ethanol. The product was dried at 80°C in vacuum oven.

6.0 g of P123 was dissolved in 45 mL of deionized water and 180 mL of 2 mol/L HCl solution with magnetic stirring at 40°C for 3 h. Then 13.0 g of TEOS was added into the above solution with stirring at 40°C for 24 h. The mixture was aged at 90°C for 24 h without stirring. The product was collected by filtration, washed with deionized water and ethanol for several times. Removal of the copolymer surfactant P123 was conducted by Soxhlet extraction with ethanol for 24 h. The product was dried at 100°C under vacuum for 12 h.

2.0 g of $Eu(Pht)_3Phen$ was completely dissolved in 80 mL of *N*, *N*-dimethyl formamide (DMF) to yield a transparent solution. 4.0 g of SBA-15 was dispersed in 200 mL of ethanol with the aid of ultra-sonication for 1 h. The $Eu(Pht)_3Phen$/DMF solution was added to the SBA-15/ethanol solution and sonicated for 1 h at room temperature. Then, DMF and ethanol were evaporated to achieve $Eu(Pht)_3Phen$/SBA-15 hybrids.

### Preparation of the Silicone Rubber Composites

The silicone rubber composites, which contained 6, 12, 18, 24, and 30 phr (parts per hundred rubber) of $Eu(Pht)_3Phen$/SBA-15 hybrids, were prepared by blending silicone rubber with $Eu(Pht)_3Phen$/SBA-15 hybrids on a two-roll mill at room temperature, and were then cured at 160°C for 6 min under the pressure of 10 MPa. The silicone rubber composites containing 2, 10 phr of $Eu(Pht)_3Phen$, 2 phr of $Eu(Pht)_3Phen$ and 4 phr of SBA-15, 10 phr of $Eu(Pht)_3Phen$ and 20 phr of SBA-15, were also prepared by the same method for comparison.

### Characterizations

The Fourier transform infrared spectra (FT-IR) were obtained by a Perkin–Elmer spectrum 100 spectrometer carried out in a range of 4000–400 $cm^{-1}$ at a resolution of 4 $cm^{-1}$. Samples for powder were prepared using the KBr pellet method.

X-ray diffraction (XRD) patterns were recorded on an X-ray diffractometer (SA-HF3, Rigaku, Japan) with Cu K$\alpha$ radiation (wavelength 0.154 nm), 40 kV and 20 mA, in transmission mode at a scan rate of 1°/min over the range 0.6–6° ($2\theta$).

Transmission electronic microscope (TEM) measures were conducted on a JEM-2100 analytical microscope operated at an accelerating voltage of 200 kV.

Scanning electronic microscope (SEM) characterizations were measured on a JEOL JSM-7401F electron microscope operated at 1 kV.

Nitrogen adsorption–desorption isotherms were measured at 77 K, using a Quantachrome Nova 4200E instrument. The surface area was obtained according to the Brunauer–Emmett–Teller (BET) method, and the pore volume was evaluated by the Barett–Joyner–Halenda (BJH) method. Before the test, the samples were outgassed at 80°C for 5 h.

The refractive index of the silicone rubber was obtained using a variable angle spectroscopic ellipsometer (W-VASE with

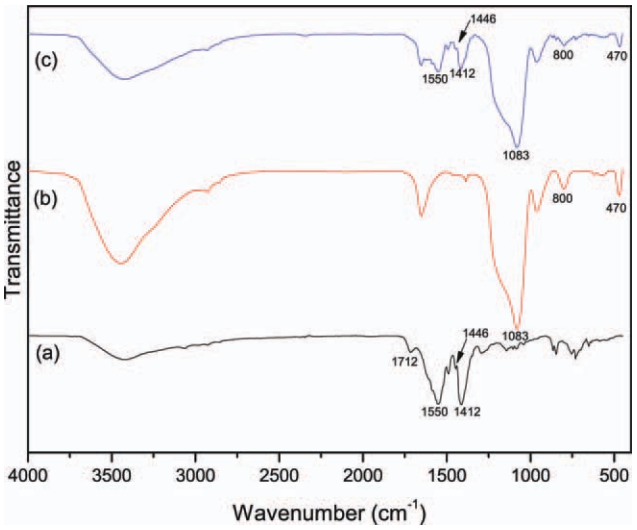


**Figure 1.** FTIR spectra of $Eu(Pht)_3Phen$ (a), SBA-15 (b), and $Eu(Pht)_3Phen$/SBA-15 hybrid (c). [Color figure can be viewed in the online issue, which is available at wileyonlinelibrary.com.]

AutoRetarder, J.A. Woollam Corp., U.S.). The data were collected in the range of 460–760 nm at 5-nm intervals.

Photoluminescence properties of the composites were measured at room temperature on a PTI QM/TM/IM steady-state and time-resolved fluorescence spectrofluorometer. The emission spectrum was monitored from 550 to 730 nm using an excitation wavelength of 265 nm. The slit width for both the excitation and emission were 1 nm. The decay curves of the composites were measured by monitoring at 615 nm from 0 to 3500 μs scanning for five times. The samples for testing were prepared to a circle sheet which was 1 mm thick and 2 cm in diameter.

## RESULTS AND DISCUSSION

### Characterizations of SBA-15 and $Eu(Pht)_3$ Phen/SBA-15 Hybrids

Figure 1 shows the FTIR spectra of the $Eu(Pht)_3Phen$, SBA-15, and $Eu(Pht)_3Phen$/SBA-15hybrid. In Figure 1(a), the adsorption band at 1712 $cm^{-1}$ was ascribed to $\nu_s$(C=O), which confirmed the existence of carboxyl groups COO-. Two peaks at 1550 and 1446 $cm^{-1}$ appear in the spectra of $Eu(Pht)_3Phen$, which was assigned to the asymmetric and symmetric vibrations of carboxyl groups $\nu_{as}$ (OCO) and $\nu_s$ (OCO), indicating the successful coordination between the oxygen atom of COO- and the $Eu^{3+}$ ions.[20] Besides, the benzene ring at 1412 $cm^{-1}$ suggested that 1,10-Phen participated in the coordination reaction.[21] In Figure 1(b), the composition of the SBA-15 was proved by the peaks at 1083 $cm^{-1}$($\nu_{as}$, Si—O), 800 $cm^{-1}$($\nu_s$, Si—O), and 470 $cm^{-1}$($\delta$, Si—O—Si).[22] In Figure 1(c), peaks which belong to the $Eu(Pht)_3Phen$ and SBA-15 were still present in the spectrum of $Eu(Pht)_3Phen$/SBA-15 hybrid, which demonstrated the successful preparation of $Eu(Pht)_3Phen$/SBA-15 hybrid.

Figure 2 displays the XRD patterns of SBA-15 and $Eu(Pht)_3Phen$/SBA-15 hybrids. Three peaks, (100), (110), and (200), of SBA-15 were still present in the pattern of $Eu(Pht)_3Phen$/SBA-15 hybrids, which demonstrated that the introduction of $Eu(Pht)_3Phen$ did not affect the mesoporous structure of SBA-15 and the long range ordered structure of SBA-15 was preserved.[11,23] The decline in diffraction intensity after the introduction of $Eu(Pht)_3Phen$ might be due to the decrease of mesoscopic order of SBA-15 and the contrast matching between the framework of SBA-15 and the organic part of $Eu(Pht)_3Phen$.[22]

SEM and TEM characterizations were carried out to investigate the morphologies and structures of SBA-15 and $Eu(Pht)_3Phen$/SBA-15 hybrids. Figure 3 shows the TEM images of SBA-15 and $Eu(Pht)_3Phen$/SBA-15 hybrids, indicating that the mesoporous structure of the SBA-15 has been preserved after the introduction of $Eu(Pht)_3Phen$, which was in agreement with the XRD data. Compared with SBA-15, as shown in the Figure 3(b), some irregular particles, which was indicated in the figure, were found on the surface of SBA-15 and the channels became dim, which was because that the $Eu(Pht)_3Phen$ was incorporated into the channels and assembled onto the surface of SBA-15.

Figure 4 displays the SEM images of SBA-15 and $Eu(Pht)_3Phen$/SBA-15 hybrids. As compared to SBA-15, $Eu(Pht)_3Phen$/SBA-15 hybrids had a slightly bigger diameter and much rougher surface as indicated in the figure, which suggested that $Eu(Pht)_3Phen$ was assembled onto the surface of the SBA-15.[24] The results were consistent with the corresponding TEM images in Figure 3.

The nitrogen adsorption–desorption isotherms of SBA-15 and $Eu(Pht)_3Phen$/SBA-15 hybrids were present in Figure 5. Both of the two samples displayed type IV isotherm curves with an H1 hysteresis at high relative pressure, characteristic of highly ordered mesoporous materials,[16] suggesting that the introduction of $Eu(pht)_3Phen$ did not affect the mesoporous structure of SBA-15, which was in agreement with the XRD and TEM data. The surface area of $Eu(Pht)_3Phen$/SBA-15 hybrids was 298 $m^2$ $g^{-1}$ calculated by BET model, much lower than that of SBA-15 (691 $m^2$ $g^{-1}$). Besides, the total pore volume was decreased from 0.83 $cm^3$ $g^{-1}$ of SBA-15 to 0.42 $cm^3$ $g^{-1}$ of $Eu(Pht)_3Phen$/SBA-15 hybrids. Both the decreases in BET area and pore

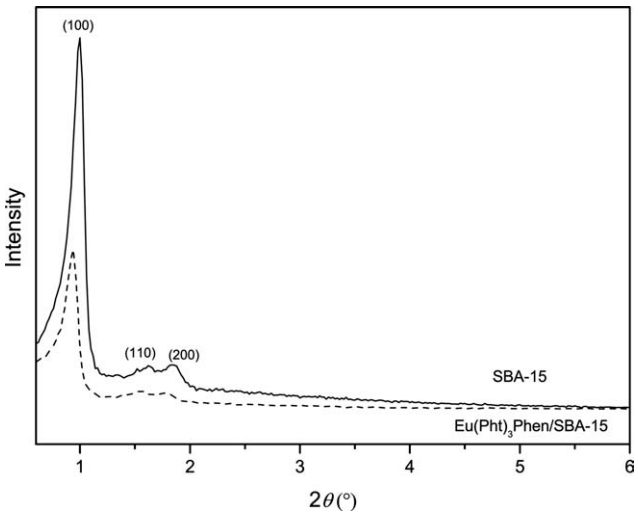


**Figure 2.** XRD patterns of SBA-15 and $Eu(Pht)_3Phen$/SBA-15 hybrids.

Applied Polymer SCIENCE

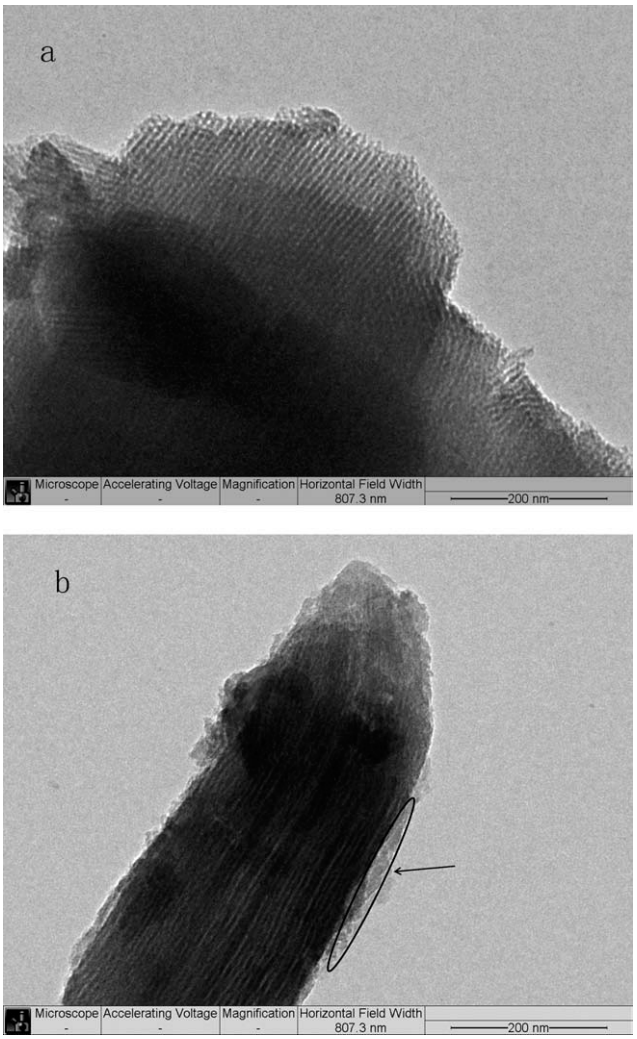


**Figure 3.** TEM images of SBA-15 (a), and Eu(Pht)$_3$Phen/SBA-15 hybrids (b).

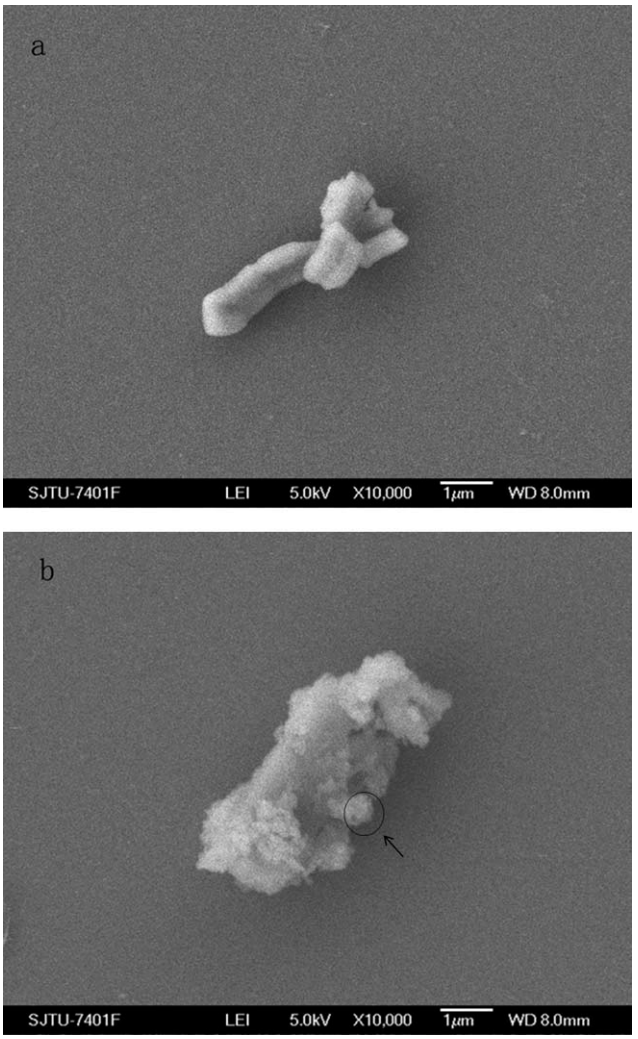


**Figure 4.** SEM images of SBA-15 (a) and Eu(pht)$_3$Phen/SBA-15 hybrids (b).

volume indicated that Eu(Pht)$_3$Phen was incorporated into the channels and assembled onto the surface of SBA-15.[22,23]

### Morphological Characterization of Silicone Rubber Composites

The dispersion, morphologies and structures of Eu(Pht)$_3$Phen, SBA-15, and Eu(Pht)$_3$Phen/SBA-15 hybrids in the silicone rubber matrix were characterized by SEM. As shown in Figure 6(a), obvious phase interface was observed between Eu(Pht)$_3$Phen and silicone rubber matrix, suggesting the weak interfacial interaction between them, thus leading to a poor disperse state of Eu(Pht)$_3$Phen in the matrix. Besides, the dimensions of the nanoparticles were pretty big and the size distribution was also not uniform, which were indicated in the figure. Figure 6(b) exhibits obvious aggregations of the Eu(Pht)$_3$Phen and SBA-15 in the silicone rubber matrix (showed in the figure with an arrow), indicating that Eu(Pht)$_3$Phen and SBA-15 were not dispersed well in the matrix. Compared with the Figure 6(a, b), there was no obvious aggregation of Eu(Pht)$_3$Phen/SBA-15 hybrids in silicone rubber matrix in Figure 6(c). As discussed above, Eu(Pht)$_3$Phen complexes were successfully incorporated

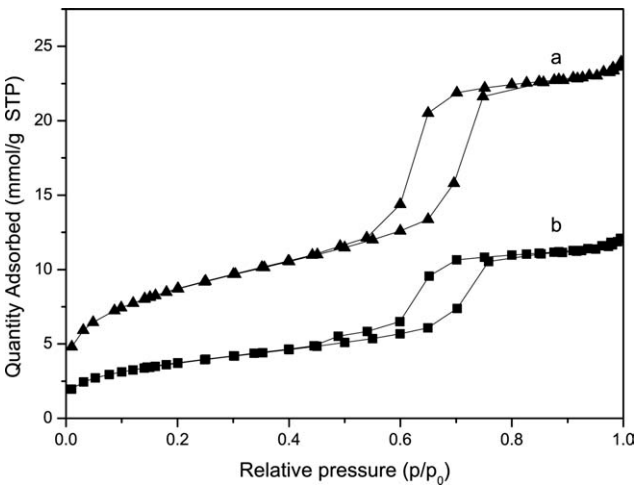


**Figure 5.** Nitrogen adsorption spectra of SBA-15 (a) and Eu(Pht)$_3$Phen/SBA-15 hybrids (b).

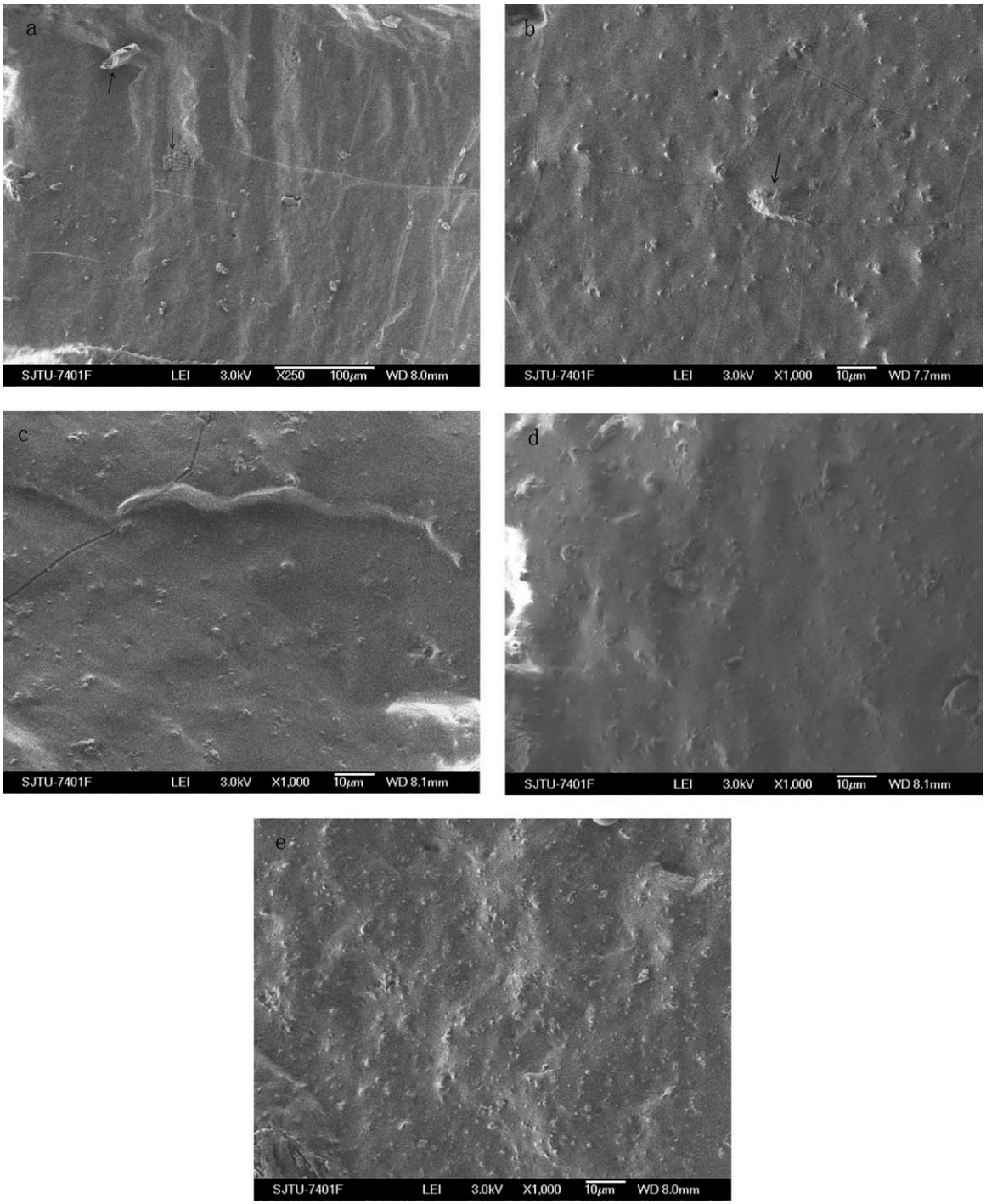


**Figure 6.** SEM images of $Eu(Pht)_3Phen$/silicone rubber composite (a-2 phr), [$Eu(Pht)_3Phen$+SBA-15]/silicone rubber composite (b-2 phr), and silicone rubber composites with $Eu(Pht)_3Phen$/SBA-15 hybrids (c-2 phr, d-6 phr, e-10 phr); All referred to the content of $Eu(Pht)_3Phen$.

into the channels and assembled onto the surface of SBA-15, the well-dispersed state of the hybrids also meants that $Eu(Pht)_3Phen$ were uniformly dispersed in the silicone rubber matrix. It facilitated the interface combination between the hybrids and the rubber matrix and reduced the energy loss of nonradiation transitions, which was favorable for enhancing the photoluminescence properties.[20] As the content of the hybrids increased to 18 and 30 phr, some aggregations were observed in the matrix, suggesting that the hybrids tend to aggregate to large particles when the content increased, which might have an adverse effect on the photoluminescence properties of the silicone rubber composites.

### Photoluminescence Properties

The photoluminescence properties of the silicone rubber composite with $Eu(Pht)_3Phen$/SBA-15 hybrids were studied. As can

Applied Polymer SCIENCE

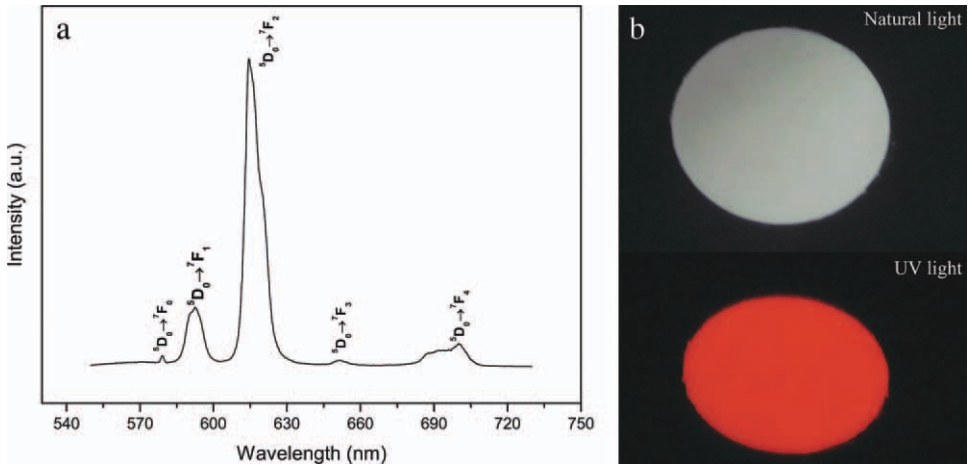


**Figure 7.** Emission spectra of the silicone rubber composite with Eu(Pht)$_3$Phen/SBA-15 hybrids (a); and the photograph of the silicone rubber composite sample under natural light and UV light (b). [Color figure can be viewed in the online issue, which is available at wileyonlinelibrary.com.]

be seen in Figure 7(a), the emission spectrum of the composite exhibited sharp emission peaks at 579, 593, 615, 650, and 701 nm, which could be attributed to $^5D_0 \rightarrow {}^7F_J$ ($J = 0$–4) transitions respectively. As shown in Figure 7(b), the composite sample showed red photoluminescence upon radiation of UV light, which was mostly attributed to the strongest transition ($^5D_0 \rightarrow {}^7F_2$) centered at 615 nm.[25,26] The $^5D_0 \rightarrow {}^7F_1$ transition is due to the magnetic dipole transition, which is insensitive to the local coordination environment of $Eu^{3+}$ ions, while the $^5D_0 \rightarrow {}^7F_2$ transition is related to electric dipole transition and sensitive to the coordination environment of the $Eu^{3+}$ ions.[25] Therefore, the integrated intensity ratio ($R$) of $^5D_0 \rightarrow {}^7F_2$ to $^5D_0 \rightarrow {}^7F_1$ ($I_{02}/I_{01}$), could indicate the asymmetry of the coordination environment of $Eu^{3+}$ ions.[27,28] The intensity at the peak of 615 nm was much stronger than that at the peak of 593 nm, indicating the low symmetry of the coordination environment of central $Eu^{3+}$ ions in the composite.[21]

As can be seen from Figure 8, the $^5D_0 \rightarrow {}^7F_2$ emission intensity of the silicone rubber composite with Eu(Pht)$_3$Phen/SBA-15 hybrids increased as the content of the hybrids increased. The photoluminescence intensity increasing rate of the composite was much higher in the content range of 6–18 phr than that of the composite in the range of 18–30 phr. It was because of the presence of the aggregations of Eu(Pht)$_3$Phen/SBA-15 hybrids as the content increased, shown in the SEM images in Figure 6(d, e), which gave birth to more energy transfer between neighboring $Eu^{3+}$ centers[18] and led to a typical emission concentration quenching, thus reducing the emission intensity.

As shown in Figure 9, when the content of Eu(Pht)$_3$Phen/SBA-15 hybrids was 6 phr (the content of Eu(Pht)$_3$Phen was 2 phr), the emission intensity at the peak of 615 nm of the silicone rubber composite with Eu(Pht)$_3$Phen/SBA-15 hybrids was 1.91 and 3.53 times higher than that of Eu(Pht)$_3$Phen/silicone rubber composite and [Eu(Pht)$_3$Phen+SBA-15]/silicone rubber composite, respectively. When the content increased to 10 phr, the photoluminescence intensity increasing ratio was 1.50 and 2.53, respectively. The improvement in photoluminescence intensity resulted from the incorporation of Eu(Pht)$_3$Phen into the channels and assembly of Eu(Pht)$_3$Phen onto the surface of the SBA-15, which improved the dispersion of Eu(Pht)$_3$Phen and inhibited aggregations of Eu(Pht)$_3$Phen at the same time. Accordingly, it also helped dilute Eu(Pht)$_3$Phen in the composite and prevented the photoluminescence concentration quenching, thus making it easy to irradiate by the excitation light and emit photoluminescence.[18] On the other hand, the SBA-15 framework enhanced the structural rigidity of the hybrids, which was helpful in reducing the energy dissipation from the nonradiative transition in the hybrids.[21] The ratios ($I_{02}/I_{01}$) of the silicone rubber composites with 6, 30 phr of Eu(Pht)$_3$Phen/SBA-15 hybrids (the content of the Eu(Pht)$_3$Phen was 2, 10 phr, respectively) were calculated to be 5.24 and 5.16, which were larger than those of Eu(Pht)$_3$Phen/silicone rubber composites (4.92 and 5.09) and [Eu(Pht)$_3$Phen+SBA-15]/silicone rubber composites (4.61 and 4.79) respectively, demonstrating that the local environment of $Eu^{3+}$ ions in the silicone rubber composite was

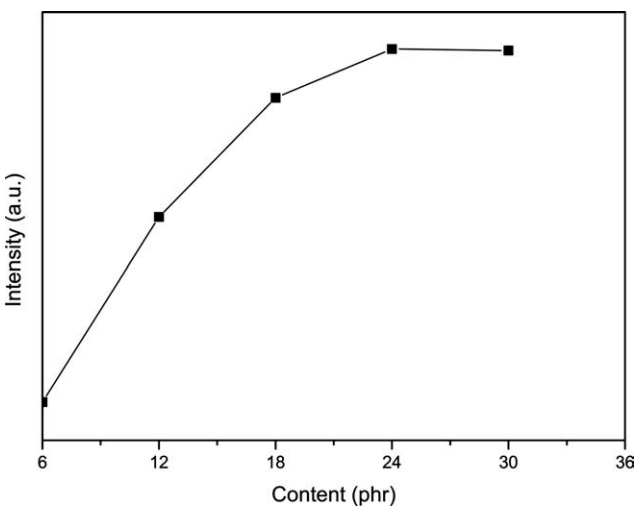


**Figure 8.** The effect of the content of Eu(Pht)$_3$Phen/SBA-15 hybrids on the $^5D_0 \rightarrow {}^7F_2$ emission intensities of the silicone rubber composites with the hybrids.

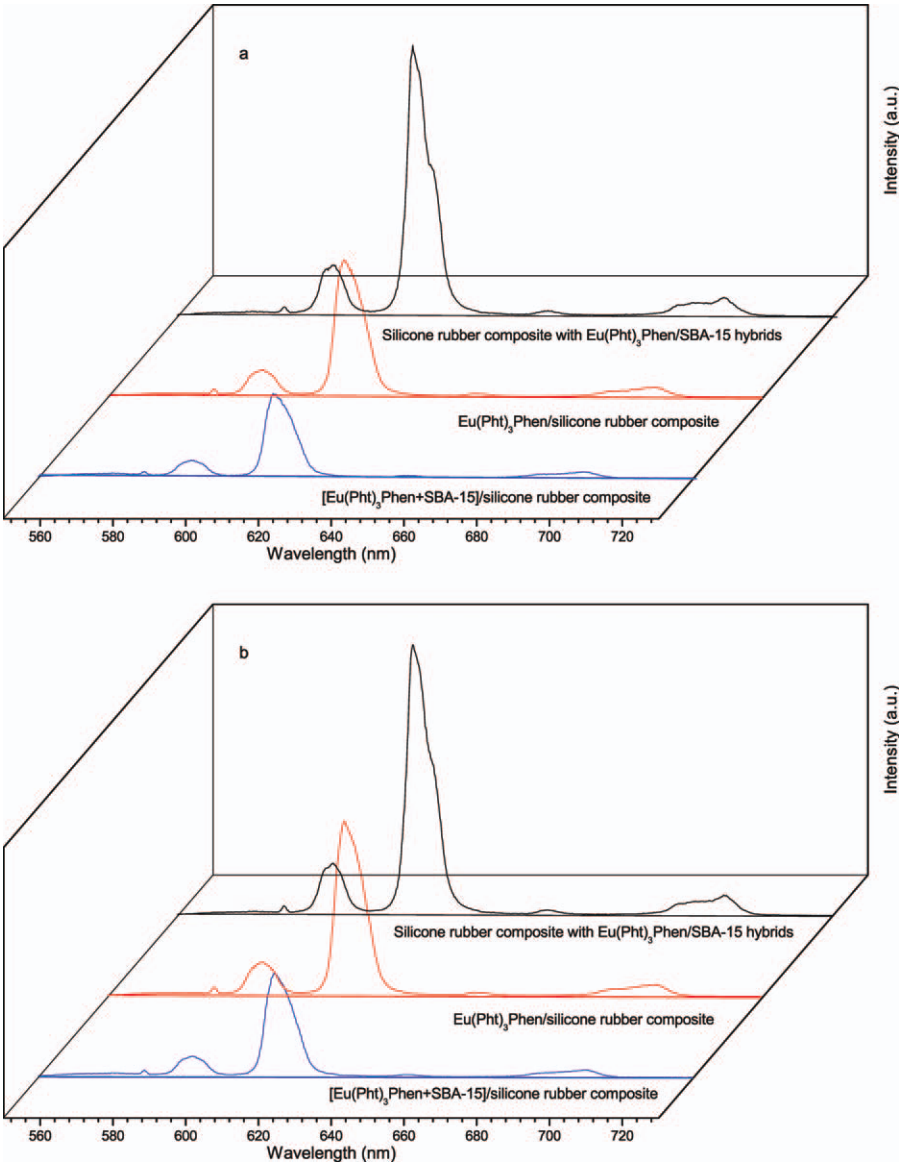


**Figure 9.** The emission spectra of the silicone rubber composites with $Eu(Pht)_3Phen$/SBA-15 hybrids, [$Eu(Pht)_3Phen$+SBA-15]/silicone rubber composites, and $Eu(Pht)_3Phen$/silicone rubber composites (a-2 phr; b-10 phr, all referred to the content of $Eu(Pht)_3Phen$). [Color figure can be viewed in the online issue, which is available at wileyonlinelibrary.com.]

much asymmetric when $Eu(Pht)_3Phen$ was incorporated into the channels and assembled onto the surface of SBA-15.[27]

The photoluminescence decay curves of $^5D_0 \rightarrow {}^7F_2$ emissions of silicone composites were obtained at room temperature, which were shown in Figure 10. The photoluminescence decay curves of all the composites could be fitted well into a mono-exponential function as $I = A \exp(-t/\tau) + I_0$, with the $R^2$ factor exceeding 0.99, confirming the presence of only one symmetric site and relatively ordered environment of $Eu^{3+}$ ions in the composites.[29,30] The lifetimes of silicone rubber composites were calculated and summarized in Table I. It was found that the lifetime of the silicone rubber composite with $Eu(Pht)_3Phen$/SBA-15 hybrids was 1035 μs, much longer than that of [$Eu(Pht)_3Phen$+SBA-15]/silicone rubber composite (902 μs) and $Eu(Pht)_3Phen$/silicone rubber composite (900 μs), which was in accordance with the above results of photoluminescence intensities. The increase in lifetime could be attributed to the rigid structure of SBA-15, effectively limiting the nonradiative vibration of the $Eu(Pht)_3Phen$,[9,31–33] thus slowing the decay rate.

### Judd-Ofelt Analysis of $Eu^{3+}$ Ions in the Silicone Rubber Composites

To investigate the local environment of the $Eu^{3+}$ ions in the silicone rubber composites, Judd-Ofelt theory was used to calculate these parameters. According to the theory, the $^5D_0 \rightarrow {}^7F_1$ transition of $Eu^{3+}$ ion is allowed by magnetic dipole, whose probability ($A_{md}$) is independent of the environment, thus it can be used as a reference.[34] While $^5D_0 \rightarrow {}^7F_{2,\ 4,\ 6}$ transitions are related

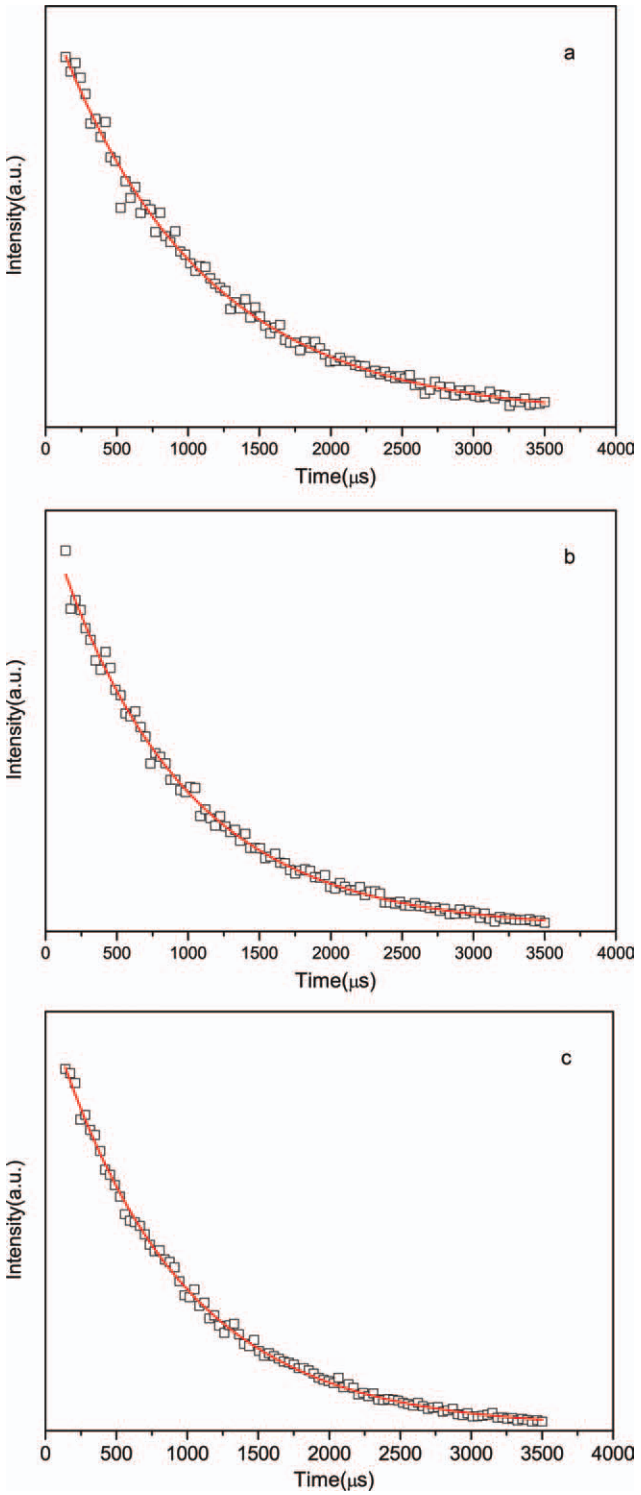


**Figure 10.** The photoluminescence decay curves of silicone rubber composites with $Eu(Pht)_3Phen/SBA-15$ hybrids (a), $[Eu(Pht)_3Phen+SBA-15]$/silicone rubber composite (b), and $Eu(Pht)_3Phen$/silicone rubber composite (c). [Color figure can be viewed in the online issue, which is available at wileyonlinelibrary.com.]

to the electric mechanisms and their radiative rates ($A_{0J}$) for $^5D_0 \rightarrow {}^7F_J$ ($J = 2, 4, 6$) transitions depend solely on intensity parameters $\Omega_2$, $\Omega_4$, and $\Omega_6$, respectively. The magnetic radiative transition probability ($A_{md}$) and electric dipole radiative transition probability ($A_{ed}$) can be calculated as follows, respectively.[34–36]

$$A_{md} = \frac{64\pi^4 \nu^3}{3h(2J+1)} n^3 S_{md} \tag{1}$$

$$\begin{aligned} A_{ed} &= \frac{64\pi^4 e^2 \nu^3}{3h(2J+1)} \frac{n(n^2+2)^2}{9} S_{ed} \\ &= \frac{64\pi^4 e^2 \nu^3}{3h(2J+1)} \frac{n(n^2+2)^2}{9} \sum_{t=2,4,6} \Omega_t \left\langle \Psi J \| U^{(t)} \| \Psi' J' \right\rangle^2 \end{aligned} \tag{2}$$

$S_{md}$ refers to the magnetic dipole line strength of the $^5D_0 \rightarrow {}^7F_1$ transition, which is $9.6 \times 10^{-42}$ $esu^2cm^2$ independent of the medium.[37] Here, $h$ is the Plank's constant, $e$ is the electronic charge, $n$ is the refractive index of the medium, silicone rubber, which was 1.40 obtained by variable angle spectroscopic ellipsometer, $\nu$ is the wavenumber of the transition, $J$ is the total angular momentum of the ground state and $J'$ is that of the final state, and $\left\langle \Psi J \| U^{(t)} \| \Psi' J' \right\rangle^2$, the square reduced matrix elements, are 0.0032, 0.0023, and 0.0002 for $t = 2$, 4, and 6, respectively.[38]

The radiative rates, $A_{0J}$ ($J = 0$–4), were calculated according to the relation with the magnetic radiative transition probability, $A_{md}$[22,39]

$$A_{0J} = A_{md} \frac{I_{0J}}{I_{md}} \frac{\nu_{md}}{\nu_{0J}} \tag{3}$$

$\nu_{md}$ and $\nu_{0J}$ are the wavenumbers of the $^5D_0 \rightarrow {}^7F_1$ and $^5D_0 \rightarrow {}^7F_J$ ($J = 0$–4) transitions, and $I_{md}$ and $I_{0J}$ are the integrated intensity of $^5D_0 \rightarrow {}^7F_1$ and $^5D_0 \rightarrow {}^7F_J$ ($J = 0$–4) transition, respectively. $A_{md}$ can be obtained by the relation with $A_{md}$ in vacuo ($(A_{md})_{vac}$), which is 14.65 $s^{-1}$.[22] The average index of refraction of the silicone rubber is 1.40, therefore, $A_{md} = n^3 (A_{md})_{vac} = 40.20\ s^{-1}$.

The $\Omega_t$ ($t = 2$, 4) can be determined from the ratios of intensities of $^5D_0 \rightarrow {}^7F_{2,4}$ transitions to the intensity of $^5D_0 \rightarrow {}^7F_1$ transition as follows.[40] The $\Omega_6$ parameter can be negligible because that the $^5D_0 \rightarrow {}^7F_6$ transition was not detected.[41]

$$\frac{A_{0J}}{A_{md}} = \frac{e^2}{S_{md}} \frac{\nu_{0J}^3}{\nu_{md}^3} \frac{(n^2+2)^2}{9n^2} \Omega_t \left\langle \Psi J \| U^{(t)} \| \Psi' J' \right\rangle^2 \tag{4}$$

**Table I.** The Lifetime, $R^2$ Factor and Standard Error Values of Silicone Rubber Composites

| Samples | τ (μs) | $R^2$ factor | Standard error |
|---|---|---|---|
| A[a] | 1035 | 0.994 | 23 |
| B | 902 | 0.996 | 16 |
| C | 900 | 0.998 | 11 |

[a]The samples A, B, and C is the silicone rubber composite with $Eu(Pht)_3Phen/SBA-15$ hybrids, $[Eu(Pht)_3Phen+SBA-15]$/silicone rubber composite, and $Eu(Pht)_3Phen$/silicone rubber composite, respectively.

**Table II.** Solid-State Spectroscopic Parameters for the $^5D_0$ Luminescence of the $Eu^{3+}$ Ions in the Silicone Rubber Composites

| Samples | $\Omega_2$ ($10^{-20}$ cm$^2$) | $\Omega_4$ ($10^{-20}$ cm$^2$) | $A_R$ (s$^{-1}$) | $A_{NR}$ (s$^{-1}$) | $\tau_{obs}$ (μs) | Φ (%) |
|---|---|---|---|---|---|---|
| A[a] | 8.902 | 2.778 | 299.301 | 666.882 | 1035 | 31.0 |
| B | 8.257 | 2.381 | 281.342 | 827.306 | 902 | 25.4 |
| C | 8.775 | 2.417 | 292.848 | 818.263 | 900 | 26.4 |

[a]The samples A, B, and C is the silicone rubber composite with $Eu(Pht)_3Phen$/SBA-15 hybrids, [$Eu(Pht)_3Phen$+SBA-15]/silicone rubber composite, and $Eu(Pht)_3Phen$/silicone rubber composite, respectively.

The calculated values of parameter $\Omega_2$ and $\Omega_4$ of silicone rubber composites were listed in Table II. $\Omega_2$ is hypersensitive to the symmetry and sequence of ligand fields and important for designing high intensity emitting materials.[42] As shown in Table II, $\Omega_2$ value of the silicone rubber composite with $Eu(Pht)_3Phen$/SBA-15 hybrids was calculated to be $8.902 \times 10^{-20}$ cm$^2$, relatively higher than that of [$Eu(Pht)_3Phen$+SBA-15]/silicone rubber composite ($8.257 \times 10^{-20}$ cm$^2$) and $Eu(Pht)_3Phen$/silicone rubber composite ($8.775 \times 10^{-20}$ cm$^2$). It indicated that the $Eu^{3+}$ ions were in highly polarizable chemical environment and demonstrated the improvement of the photoluminescence properties in the silicone rubber composite with $Eu(Pht)_3Phen$/SBA-15 hybrids,[22] which was in accordance with the results of the photoluminescence intensities in Figure 8(b). $\Omega_4$ values, corresponding to the intensity of $^5D_0 \rightarrow {}^7F_4$ transition, are related to the bulk properties of the hosts, while no theoretical prediction was found for this sensibility to macroscopic properties.[34,43]

The luminescent quantum efficiency (Φ) for the $^5D_0 \rightarrow {}^7F_{0\text{-}4}$ transitions of $Eu^{3+}$ ions fundamentally determines the luminescent properties of the composites, and can be determined on the basis of the emission spectra and lifetime of $^5D_0$ excited state. Φ is defined and calculated according to eqs. (5)–(7).[11,22,24,39,44]

$$\Phi = \frac{A_R}{A_R + A_{NR}} \tag{5}$$

$A_R$ is the radiative transition rate, which can be calculated by summing all the radiative rates $A_{0J}$ for each $^5D_0 \rightarrow {}^7F_J$ ($J = 0$–4) transition.

$$A_R = A_{md} \sum_{\lambda} \frac{I_{0J}}{I_{md}} \frac{v_{md}}{v_{0J}} \tag{6}$$

$A_{NR}$ is the nonradiative transition rate and can be obtained by the relation with the lifetime observed ($\tau_{obs}$) and radiative transition rate ($A_R$).

$$\tau_{obs} = \frac{1}{A_R + A_{NR}} \tag{7}$$

The values of $A_R$, $A_{NR}$, and Φ of silicone rubber composites were calculated by the above equations, and results were listed in Table II. It was found that the photoluminescence quantum efficiency of the silicone rubber composite with $Eu(Pht)_3Phen$/SBA-15 hybrids was 31.0%, relatively higher than that of [$Eu(Pht)_3Phen$+SBA-15]/silicone rubber composite (25.4%) and $Eu(Pht)_3Phen$/silicone rubber composite (26.4%). This phenomenon could be attributed to the rigid structure of SBA-15, which could reduce the nonradiative transition rates caused by vibration of the $Eu^{3+}$ ions.[45] On the other hand, $Eu(Pht)_3Phen$/SBA-15 hybrids were uniformly dispersed in silicone rubber composites, thus reducing the energy transfer among $Eu(Pht)_3Phen$ nanoparticles[27] and leading to a higher photoluminescence quantum efficiency.

## CONCLUSIONS

$Eu(Pht)_3Phen$/SBA-15 hybrids were prepared and their morphologies and structures were characterized by XRD, nitrogen adsorption–desorption, SEM and TEM, which proved that $Eu(Pht)_3Phen$ was successfully incorporated into the channels and assembled onto the surface of SBA-15. The silicone rubber composites with various contents of $Eu(Pht)_3Phen$/SBA-15 hybrids were prepared and their photoluminescence properties were also studied. The results showed that the photoluminescence intensities of the composites with the hybrids increased as the content of the hybrids increased and higher than those of $Eu(Pht)_3Phen$/silicone rubber composites and [$Eu(Pht)_3Phen$+SBA-15]/silicone rubber composites when the content of $Eu(Pht)_3Phen$ was equal. Besides, the photoluminescence decay curves of the composites showed that the lifetime of the silicone rubber composite with $Eu(Pht)_3Phen$/SBA-15 hybrids was 1035 μs, much longer than that of $Eu(Pht)_3Phen$/silicone rubber composite (900 μs) and [$Eu(Pht)_3Phen$+SBA-15]/silicone rubber composite (902 μs). According to the results calculated by Judd-Ofelt theory, the $Eu^{3+}$ ions in the composite with the hybrids occupied more asymmetrical environment and the photoluminescence quantum efficiency (31.0%) was relatively higher compared to the $Eu(Pht)_3Phen$/silicone rubber composite (26.4) and [$Eu(Pht)_3Phen$+SBA-15]/silicone rubber composite (25.4%) due to the rigid framework structure of SBA-15 which reduced the nonradiative transition rate and the improvement of the dispersion of hybrids in the composites.

## REFERENCES


1. Prokhorov, A. M.; Kozhevnikov, V. N.; Kopchuk, D. S.; Bernard, H.; Le Bris, N.; Tripier, R.; Handel, H.; Koenig, B.; Kozhevnikov, D. N. *Tetrahedron* **2011,** *67*, 597.
2. Zhang, J.; Fu, Y.; Lakowicz, J. R. *J. Phys. Chem. C 113*, 19404 **2009.**
3. Ocaña, M.; Cantelar, E.; Cussó, F. *Mater. Chem. Phys.* **2011,** *125*, 224.

4. Guo, L.; Wu, S.; Zeng, F.; Zhao, J. *Eur. Polym. J.* **2006,** *42*, 1670.
5. Jiang, H.; Wang, G.; Zhang, W.; Liu, X.; Ye, Z.; Jin, D.; Yuan, J.; Liu, Z. J. *Fluoresc.* **2010,** *20*, 321.
6. Armelao, L.; Bottaro, G.; Bovo, L.; Maccato, C.; Pascolini, M.; Sada, C.; Soini, E.; Tondello, E. *J. Phys. Chem. C* **2009,** *113*, 14429.
7. Lezhnina, M.; Benavente, E.; Bentlage, M.; Echevarria, Y.; Klumpp, E.; Kynast, U. *Chem. Mater.* **2007,** *19*, 1098.
8. Qiao, Y.; Chen, H.; Lin, Y.; Yang, Z.; Cheng, X.; Huang, J. *J. Phys. Chem. C* **2011,** *115*, 7323.
9. Wang, Y.; Li, B.; Zhang, L.; Zuo, Q.; Liu, L.; Li, P. *J. Colloid Interface Sci.* **2010,** *349*, 505.
10. Xu, Q.; Li, L.; Liu, X.; Xu, R. *Chem. Mater.* **2002,** *14*, 549.
11. Li, Y.-J.; Yan, B.; Li, Y. *Microporous Mesoporous Mater.* **2010,** *131*, 82.
12. Peng, C.; Zhang, H.; Meng, Q.; Li, H.; Yu, J.; Guo, J.; Sun, L. *Inorg. Chem. Commun.* **2005,** *8*, 440.
13. Fu, L.; Xu, Q.; Zhang, H.; Li, L.; Meng, Q.; Xu, R. *Mater. Sci. Eng. B* **2002,** *88*, 68.
14. Bruno, S. M.; Coelho, A. C.; Ferreira, R. A. S.; Carlos, L. D.; Pillinger, M.; Valente, A. A.; Ribeiro-Claro, P.; Gonçalves, I. S. *Eur. J. Inorg. Chem.* **2008,** *3786*, 2008.
15. Zhao, D.; Feng, J.; Huo, Q.; Melosh, N.; Fredrickson, G. H.; Chmelka, B. F.; Stucky, G. D. *Science* **1998,** *279*, 548.
16. Kruk, M.; Jaroniec, M.; Joo, S. H.; Ryoo, R. *J. Phys. Chem. B* **2003,** *107*, 2205.
17. Liu, L.; Lu, Y. L.; He, L.; Zhang, W.; Yang, C.; Liu, Y. D.; Zhang, L. Q.; Jin, R. G. *Adv. Funct. Mater.* **2005,** *15*, 309.
18. Wen, S.; Zhang, X.; Hu, S.; Zhang, L.; Liu, L. *Polymer* **2009,** *50*, 3269.
19. Liu, L.; Zhang, W.; Li, X.; Wu, X.; Yang, C.; Liu, Y.; He, L.; Lu, Y.; Xu, R.; Zhang, X. *Compos. Sci. Technol.* **2007,** *67*, 2199.
20. Yang, C.; Liu, L.; Lu, Y.; He, L.; Zhang, W.; Zhang, L. *J. Appl. Polym. Sci.* **2005,** *96*, 20.
21. Wan, C.; Li, M.; Bai, X.; Zhang, Y. *J. Phys. Chem. C* **2009,** *113*, 16238.
22. Peng, C.; Zhang, H.; Yu, J.; Meng, Q.; Fu, L.; Li, H.; Sun, L.; Guo, X. *J. Phys. Chem. B* **2005,** *109*, 15278.
23. Geng, W.; Li, X.; Li, N.; Zhang, T.; Wang, W.; Qiu, S. *J. Appl. Polym. Sci.* **2006,** *102*, 3301.
24. Li, Y.; Yan, B.; Li, Y. *J. Solid State Chem.* **2010,** *183*, 871.
25. Yang, L.; Zhou, L.; Huang, Y.; Tang, Z. *Mater Res. Bull.* **2011,** *46*, 239.
26. Liu, P.; Li, H.; Wang, Y.; Liu, B.; Zhang, W.; Wang, Y.; Yan, W.; Zhang, H.; Schubert, U. *J. Mater. Chem.* **2008,** *18*, 735.
27. Zhang, X.; Wen, S.; Hu, S.; Chen, Q.; Fong, H.; Zhang, L.; Liu, L. *J. Phys. Chem. C* **2010,** *114*, 3898.
28. Wang, X.; Chen, J.; Li, J.; Guo, H. *J. Non-Cryst. Solids* **2011,** *357*, 2290.
29. Liu, S.; He, P.; Wang, H.; Shi, J.; Gong, M. *J. Lumin* **2010,** *130*, 855.
30. Li, H. R.; Lin, J.; Zhang, H. J.; Li, H. C.; Fu, L. S.; Meng, Q. G. *Chem. Commun.* **2001,** *13*, 1212.
31. Milanova, M.; Zaharieva, J.; Manolov, I.; Getzova, M.; Todorovsky, D. *J. Rare Earth* **2010,** *28*, 66.
32. Chen, Y.; Chen, Q.; Song, L.; Li, H.-P.; Hou, F.-Z. J. *Lumin* **2009,** *129*, 867.
33. Guo, J. *Mater. Lett.* **2003,** *57*, 3899.
34. Xie, F.; Liang, H.; Chen, B.; Xu, J.; Guo, F. *J. Mater. Sci.* **2009,** *45*, 405.
35. Ebendorff-Heidepriem, H.; Ehrt, D. *J. Non-Cryst. Solids* **1996,** *208*, 205.
36. Liu, L.; Chen, X. *Nanotechnology* **2007,** *18*, 255704.
37. Werts, M. H. V.; Jukes, R. T. F.; Verhoeven, J. W. *Phys. Chem. Chem. Phys.* **2002,** *4*, 1542.
38. Liang, H.; Xie, F. *Adv. Mater. Res.* **2011,** *233*, 1227.
39. Yan, B.; Qiao, X. F. *J. Phys. Chem. B* **2007,** *111*, 12362.
40. Babu, P.; Jayasankar, C. *Physica B* **2000,** *279*, 262.
41. Liang, H.; Zhang, Q.; Zheng, Z.; Ming, H.; Li, Z.; Xu, J.; Chen, B.; Zhao, H. *Opt. Lett.* **2004,** *29*, 477.
42. Hasegawa, Y.; Yamamuro, M.; Wada, Y.; Kanehisa, N.; Kai, Y.; Yanagida, S. *J. Phys. Chem. A* **2003,** *107*, 1697.
43. Liang, H.; Xie, F. *Spectrochim. Acta A Mol. Biomol. Spectrosc.* **2010,** *77*, 348.
44. Fan, W.; Feng, J.; Song, S.; Lei, Y.; Dang, S.; Zhang, H. *Opt. Mater.* **2011,** *33*, 582.
45. Liang, H.; Xie, F.; Liu, M.; Jin, Z.; Luo, F.; Zhang, Z. *Spectrochim. Acta A Mol. Biomol. Spectrosc.* **2008,** *71*, 588.